Journal of Mathematical Imaging and Vision manuscript No.
(will be inserted by the editor)

On Numerical Analysis of View Dependent Derivatives in Computed Tomography

Adel Faridani · **Ryan Hass**

Received: June 30, 2014 / Accepted: February 3, 2015

Abstract We explore the numerical implementation of a view dependent derivative that occurs in π-line reconstruction formulas for two- and three-dimensional computed tomography. Focusing on two-dimensional fan-beam tomography we provide an error analysis and a common framework for the comparison of several schemes used to discretize this derivative. The leading error terms for each scheme are determined. The results demonstrate some advantages and drawbacks of the methods that are confirmed by numerical experiments.

Keywords tomography · fan-beam · π-line · filtered back projection

1 Introduction

In x-ray tomography one measures the attenuation of an x-ray beam that passes through the object. If scatter can be neglected, the mathematical model is given by the divergent beam transform

$$\mathscr{D}f(\mathbf{y},\theta) = \int_0^\infty f(\mathbf{y}+t\theta)\,dt.$$

The function f is the x-ray attenuation coefficient of the object, the point $\mathbf{y}$ is the position of the x-ray source and the unit vector θ gives the direction of the ray. We assume a mode of data acquisition where the the x-ray source moves on a curve $\mathbf{y} = \mathbf{y}(s)$, the most common choice being a circle. Work on inversion formulas and efficient reconstruction methods goes

Part of this research was supported by NSF grant DMS-0709495.

A. Faridani
Department of Mathematics
Oregon State University
Corvallis, OR 97331
Tel.: +1-541-737-5182
Fax: +1-541-737-0517
E-mail: faridani@math.oregonstate.edu

R. Hass
Department of Mathematics
Oregon State University
Corvallis, OR 97331
E-mail: hassr@math.oregonstate.edu

back to the early days of tomography and the standard methods and algorithms developed in these early decades have been summarized in monographs such as [7,12,14]. A more recently developed class of inversion formulas that are valid in both two and three-dimensions are π-line reconstruction formulas [1,4,8–10,15,16,21–23]. Fan-beam reconstruction algorithms based on π-line formulas have some advantages over the classical algorithms as they do not need certain approximations, and such an algorithm has been given as the fan-beam method of choice in the more recent textbook [8]. These algorithms all include a certain derivative, taken with respect to the source position while the direction of the ray is held constant, namely

$$\frac{\partial}{\partial q}\mathscr{D}f(\mathbf{y}(q),\theta)\bigg|_{q=s}. \tag{1}$$

In particular the derivative is present in the reconstruction formula

$$f(\mathbf{x}) = \frac{-1}{2\pi^2}\int_{I_\pi(\mathbf{x})}\frac{1}{|\mathbf{x}-\mathbf{y}(s)|}\int_0^{2\pi}\frac{\partial}{\partial q}\mathscr{D}f(\mathbf{y}(q),\theta(s,x,\gamma))\bigg|_{q=s}\frac{d\gamma}{\sin\gamma}ds \tag{2}$$

found in [10], which is used for the numerical experiments presented below. Here $I_\pi(\mathbf{x}) = [s_b(\mathbf{x}), s_t(\mathbf{x})]$ is such that $\mathbf{y}(s_b(\mathbf{x}))$, $\mathbf{y}(s_t(\mathbf{x}))$, and $\mathbf{x}$ are collinear. This paper is concerned with the numerical implementation of (1). Geometrically, the derivative can be understood as the difference quotient of x-ray data from parallel lines that pass through the object. However the fan-beam scanning geometry does not directly make measurements over parallel lines. As a result, a direct implementation of the derivative provides poor results and efforts have been made to overcome this limitation. Initially the derivative was considered to be unfavorable because it can reduce tangential resolution in the reconstruction [20], and the early implementation schemes reduced the competitiveness of the π-line reconstruction algorithm compared to other reconstruction methods. The derivative can be removed by an integration by parts [5,9]. However this choice increases the computational complexity of the numerical inversion in the 3D case [17].

The paper is organized as follows. As there is considerable flexibility both with regard to the choice of source curve and the corresponding detector geometry, we use the next section to review some common set-ups. In section 3 a number of numerical schemes to implement (1) are described. Our detailed theoretical analysis is focused on a circular source curve and curved detector geometry. For this set-up, we compare the schemes in a common framework and discuss the main results in section 4, deferring the derivations to section 5. Numerical experiments are presented and discussed as well. Section 5 is devoted to the derivation of the leading error terms for each scheme and conclusions are presented in section 6.

2 Detector geometries

In this section we briefly describe some fan-beam data acquisition geometries. The available data are discrete samples of the divergent beam transform $\mathscr{D}f(\mathbf{y},\theta)$ for certain values of $\mathbf{y}$ and θ. We assume that the source positions $\mathbf{y}$ lie on a given curve $\mathbf{y}(s)$. In order to describe some common data acquisition geometries we follow the approach of [17] , while keeping notation consistent with our own earlier work [3,4], and associate with each given s a pair $\mathbf{e}_u(s), \mathbf{e}_v(s)$ of mutually orthogonal unit vectors. Here $\mathbf{e}_v$ corresponds to $-\mathbf{e}_w$ in [17]. Let D denote the distance of the source position $\mathbf{y}(s)$ to the center of the detector array. D is assumed to be constant. The center of the detector array is at the location $\mathbf{y}(s) + D\mathbf{e}_v(s)$.

If the detector array is linear (flat detectors) then detectors are positioned along the line at locations

$$\mathbf{d}_f(s,u) = \mathbf{y}(s) + D\,\mathbf{e}_v(s) + u\,\mathbf{e}_u(s), \quad u \in \mathbf{R}. \tag{3}$$

In this case u is the signed distance of the detector position to the center of the linear detector array and the direction θ of a measured ray can be parametrized as

$$\theta \;=\; \theta(s,u) \;=\; \frac{\mathbf{d}_f(s,u) - \mathbf{y}(s)}{|\mathbf{d}_f(s,u) - \mathbf{y}(s)|} \;=\; \frac{u\mathbf{e}_u(s) + D\mathbf{e}_v(s)}{\sqrt{D^2+u^2}}. \tag{4}$$

If the detectors are located on a circular arc (curved detector array), then detectors are positioned at

$$\mathbf{d}_c(s,u) = \mathbf{y}(s) + D\cos(u)\mathbf{e}_v(s) + D\sin(u)\mathbf{e}_u(s), \quad -\frac{\pi}{2} < u < \frac{\pi}{2}.$$

The direction θ of the measured ray is then given by

$$\theta \;=\; \theta(s,u) \;=\; \frac{\mathbf{d}_c(s,u) - \mathbf{y}(s)}{|\mathbf{d}_c(s,u) - \mathbf{y}(s)|} \;=\; \sin(u)\mathbf{e}_u(s) + \cos(u)\mathbf{e}_v(s).$$

Here u denotes the acute angle between the position vector $\mathbf{y}(s)$ and the direction θ of the ray.

In general we assume that θ is parametrized as

$$\theta(s,u) = c_1(u)\,\mathbf{e}_u(s) \;+\; c_2(u)\,\mathbf{e}_v(s), \quad c_1^2(u) + c_2^2(u) = 1 \tag{5}$$

and that $c_1(u)$ is differentiable and admits an inverse function $c_1^{-1}(u)$ for the relevant interval of values for u. It follows that u can be expressed in terms of s and θ by

$$u(s,\theta) = c_1^{-1}(\theta \cdot \mathbf{e}_u(s)). \tag{6}$$

Let

$$g(s,u) = \mathscr{D}f(\mathbf{y}(s), \theta(s,u)).$$

Now the view dependent derivative (1) can be written as

$$\begin{aligned} \frac{d}{dq}\mathscr{D}f(\mathbf{y}(q),\theta)\bigg|_{q=s} \;&=\; \frac{d}{dq}g(q,u(q,\theta))\bigg|_{q=s} \\ &= \frac{\partial g}{\partial s}(s,u(s,\theta)) \;+ \frac{\partial g}{\partial u}(s,u(s,\theta))\frac{\partial u(s,\theta)}{\partial s}. \end{aligned} \tag{7}$$

Since $\| \mathbf{e}_u(s) \| = 1$, $\mathbf{e}_u(s)$ and its derivative $\mathbf{e}'_u(s)$ are always mutually orthogonal. Furthermore, the orthogonality of $\mathbf{e}_u(s)$ and $\mathbf{e}_v(s)$ for all s implies $\mathbf{e}'_u(s)\cdot\mathbf{e}_v(s) = -\mathbf{e}_u(s)\cdot\mathbf{e}'_v(s)$. Together with (5) one obtains

$$\theta\cdot\mathbf{e}'_u(s) \;=\; c_2(u(s,\theta))\mathbf{e}'_u(s)\cdot\mathbf{e}_v(s) \;=\; -c_2(u(s,\theta)\mathbf{e}_u(s)\cdot\mathbf{e}'_v(s).$$

Using this and (6) gives

$$\begin{aligned} \frac{\partial u(s,\theta)}{\partial s} &= \frac{\partial}{\partial s}c_1^{-1}(\theta\cdot\mathbf{e}_u(s)) \\ &= \frac{\theta\cdot\mathbf{e}'_u(s)}{c'_1(c_1^{-1}(\theta\cdot\mathbf{e}_u(s)))} \\ &= \frac{-c_2(u(s,\theta))}{c'_1(u(s,\theta))}\mathbf{e}_u(s)\cdot\mathbf{e}'_v(s) \end{aligned} \tag{8}$$

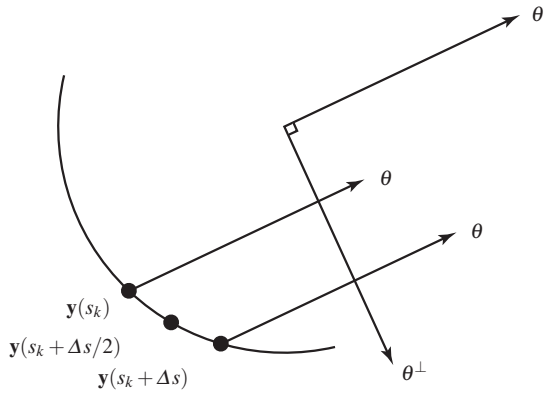

Fig. 1 The direction $\theta = \theta(s_{k+\frac{1}{2}}, u_i)$ used in the direct scheme.

For the curved detector array one has $c_1(u) = \sin(u)$, $c_2(u) = \cos(u)$ and (8) reads

$$\frac{\partial u(s,\theta)}{\partial s} = -\mathbf{e}_u(s) \cdot \mathbf{e}'_v(s) \tag{9}$$

For the flat detector array $c_1(u) = u/\sqrt{D^2+u^2}$, $c_2(u) = D/\sqrt{D^2+u^2}$, and

$$\frac{\partial u(s,\theta)}{\partial s} = -\frac{D^2 + (u(s,\theta))^2}{D} \mathbf{e}_u(s) \cdot \mathbf{e}'_v(s) \tag{10}$$

3 Difference schemes

In this section we introduce the difference schemes that we will analyze. We assume that the data $g(s,u) = \mathscr{D}f(\mathbf{y}(s), \theta(s,u))$ have been measured at points (s_k, u_i) with $s_k = k\Delta s$ and $u_i = i\Delta u$. We will use the notations $g_{k,i} = g(s_k, u_i)$, $s_{k\pm\frac{1}{2}} = s_k \pm \frac{1}{2}\Delta s$, and $u_{i\pm\frac{1}{2}} = u_i \pm \frac{1}{2}\Delta u$. Let $g'(s,u)$ denote the desired view dependent derivative

$$g'(s,u) = \frac{d}{dq} \mathscr{D}f(\mathbf{y}(q), \theta(s,u))\Big|_{q=s}. \tag{11}$$

For some schemes linear interpolation of the measured data in u will be used. Throughout this paper let $\mathscr{I}g$ denote linear interpolation of g in the second variable, that is

$$\mathscr{I}g(s,u) = cg(s,u_i) + (1-c)g(s,u_{i+1}) \tag{12}$$

with i such that $u_i \le u < u_{i+1}$ and $c = (u_{i+1} - u)/\Delta u$.

3.1 The direct scheme

The direct scheme is a straightforward discretization of (11):

$$\begin{aligned} & g'(s_{k+\frac{1}{2}}, u_i) \simeq g'_{\text{dir}}(s_{k+\frac{1}{2}}, u_i) \\ &= \frac{1}{\Delta s}\left(\mathscr{D}f(\mathbf{y}(s_{k+1}), \theta(s_{k+\frac{1}{2}}, u_i)) - \mathscr{D}f(\mathbf{y}(s_k), \theta(s_{k+\frac{1}{2}}, u_i))\right) \\ &= \left(g(s_{k+1}, \tilde{u}_1) - g(s_k, \tilde{u}_0)\right)/\Delta s \end{aligned}$$

with

$$\tilde{u}_0 = c_1^{-1}(\theta(s_{k+\frac{1}{2}}, u_i)\cdot e_u(s_k)), \quad \tilde{u}_1 = c_1^{-1}(\theta(s_{k+\frac{1}{2}}, u_i)\cdot e_u(s_{k+1})). \tag{13}$$

Since the data $g(s,u)$ are in general not measured at the required points $(s_{k+1}, \tilde{u}_1)$ and $(s_k, \tilde{u}_0)$, linear interpolation in u is used. So the direct scheme reads

$$g'_{\text{dir}}(s_{k+\frac{1}{2}}, u_i) = (\mathscr{I}g(s_{k+1}, \tilde{u}_1) - \mathscr{I}g(s_k, \tilde{u}_0))/\Delta s \tag{14}$$

with $\tilde{u}_0$, $\tilde{u}_1$ given by (13).

3.2 The Noo-Pack-Heuscher (NPH) scheme

This scheme was suggested by Noo, Pack, and Heuscher [18] as an improvement over the direct scheme which had shown in numerical experiments to yield suboptimal resolution (see, e.g., [17, Fig. 3]). This scheme is a discretization of (7) and reads

$$\begin{aligned} & g'(s_{k+\frac{1}{2}}, u_{i+\frac{1}{2}}) \simeq g'_{\text{NPH}}(s_{k+\frac{1}{2}}, u_{i+\frac{1}{2}}) \\ = \; & \frac{\left[(g_{k+1,i+1} - g_{k,i+1}) + (g_{k+1,i} - g_{k,i})\right]}{2\Delta s} \\ & + \frac{\partial u}{\partial s}(s_{k+\frac{1}{2}}, \theta(s_{k+\frac{1}{2}}, u_{i+\frac{1}{2}}))\frac{\left[(g_{k+1,i+1} - g_{k+1,i}) + (g_{k,i+1} - g_{k,i})\right]}{2\Delta u} \\ \text{with } & \frac{\partial u}{\partial s}(s_{k+\frac{1}{2}}, \theta(s_{k+\frac{1}{2}}, u_{i+\frac{1}{2}})) = \frac{-c_2(u_{i+\frac{1}{2}})}{c_1'(u_{i+\frac{1}{2}})}\mathbf{e}_u(s_{k+\frac{1}{2}})\cdot\mathbf{e}_v'(s_{k+\frac{1}{2}}) \end{aligned} \tag{15}$$

where the last equation follows from (8). The NPH scheme was the accepted standard for a few years but it was observed that it has non-isotropic resolution, see, e.g., [20]. We will discuss this point further in the next section. The following three schemes are attempts to remedy this drawback.

3.3 The Noo-Hoppe-Dennerlein-Lauritsch-Hornegger (NHDLH) scheme

This ingenious scheme was proposed in [17] as an improvement over the NPH scheme and is currently considered the most robust with respect to a variety of data acquisition geometries. Its starting point is a formula similar to the direct scheme but with a free parameter ε, $0 < \varepsilon < 1$. Let $\theta = \theta(s_k, u_{i+\frac{1}{2}})$. Then

$$g'(s_k, u_{i+\frac{1}{2}}) \simeq \frac{\mathscr{D}f(\mathbf{y}(s_k + \varepsilon\Delta s), \theta) - \mathscr{D}f(\mathbf{y}(s_k - \varepsilon\Delta s), \theta)}{2\varepsilon\Delta s}. \tag{16}$$

Interpolation is needed to implement (16) since the required values of $\mathscr{D}f$ are in general not being measured. The following interpolation step is original and a core idea of this scheme. Approximate

$$\mathscr{D}f(\mathbf{y}(s_k + \varepsilon\Delta s), \theta) \simeq (1-\varepsilon)g(s_k, \nu_+) + \varepsilon g(s_{k+1}, \mu_+) \tag{17}$$

$$\mathscr{D}f(\mathbf{y}(s_k - \varepsilon\Delta s), \theta) \simeq (1-\varepsilon)g(s_k, \nu_-) + \varepsilon g(s_{k-1}, \mu_-) \tag{18}$$

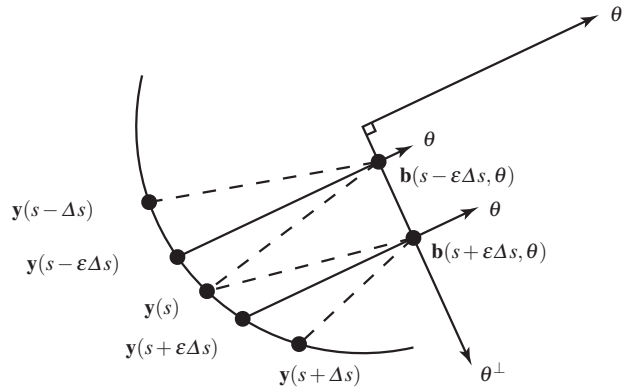

Fig. 2 The NHDLH scheme. $s = s_k$, $\theta = \theta(s_k, u_{i+\frac{1}{2}})$, and $\mathbf{b}(t,\theta) = \mathbf{y}(t) - (\mathbf{y}(t)\cdot\theta)\theta$. The dashed lines represent $g(s,\nu_\pm)$, $g(s+\Delta s,\mu_+)$, and $g(s-\Delta s,\mu_-)$, respectively.

The idea is to introduce a 'point of interest' $\mathbf{b}(t,\theta) = \mathbf{y}(t) - (\mathbf{y}(t)\cdot\theta)\theta$ with $\theta = \theta(s_k, u_{i+\frac{1}{2}})$. Then $g(s_k,\nu_\pm)$ corresponds to the lines connecting $\mathbf{y}(s_k)$ with $\mathbf{b}(s_k \pm \varepsilon\Delta s,\theta)$, respectively; cf. the dashed lines with vertex $\mathbf{y}(s)$ in Figure 2. Similarly, $g(s_{k-1},\mu_-)$ corresponds to the line connecting $\mathbf{y}(s_{k-1})$ with $\mathbf{b}(s_k - \varepsilon\Delta s,\theta)$, and $g(s_{k+1},\mu_+)$ to the line connecting $\mathbf{y}(s_{k+1})$ with $\mathbf{b}(s_k + \varepsilon\Delta s,\theta)$.

Inserting (17) and (18) into (16) and using linear interpolation in u for the $g(s_k,\nu_\pm)$ and $g(s_{k\pm1},\mu_\pm)$ gives

$$\begin{aligned} & g'(s_k, u_{i+\frac{1}{2}}) \simeq g'_{\mathrm{NHDLH}}(s_k, u_{i+\frac{1}{2}}) \\ &= \frac{\mathscr{I}g(s_{k+1},\mu_+) - \mathscr{I}g(s_{k-1},\mu_-)}{2\Delta s} + (1-\varepsilon)\frac{\mathscr{I}g(s_k,\nu_+) - \mathscr{I}g(s_k,\nu_-)}{2\varepsilon\Delta s} \end{aligned} \tag{19}$$

3.4 The Faridani-Hass-Solmon (FHS) scheme

The FHS scheme was suggested in [3] for the curved detector geometry as an improvement over the NPH scheme and a simple alternative to the NHDLH scheme. Like the NPH scheme it is based on a discretization of (7). It was observed in [3] that the non-isotropic resolution of the NPH scheme comes from averaging two slightly rotated images. This effect comes from averaging the numerical derivatives with respect to u at source positions s_k and s_{k+1} in (15). The FHS scheme avoids this averaging at the cost of increasing the stepsize for the differentiation in s. The general form of the FHS scheme reads

$$\begin{aligned} & g'(s_k, u_{i+\frac{1}{2}}) \simeq g'_{\mathrm{FHS}}(s_k, u_{i+\frac{1}{2}}) \\ &= \frac{\left[(g_{k+1,i} - g_{k-1,i}) + (g_{k+1,i+1} - g_{k-1,i+1})\right]}{4\Delta s} \\ &\quad + \frac{\partial u}{\partial s}(s_k, \theta(s_k, u_{i+\frac{1}{2}}))\,\frac{g_{k,i+1} - g_{k,i}}{\Delta u} \end{aligned} \tag{20}$$

$$\text{with } \frac{\partial u}{\partial s}(s_k, \theta(s_k, u_{i+\frac{1}{2}})) = \frac{-c_2(u_{i+\frac{1}{2}})}{c_1'(u_{i+\frac{1}{2}})}\mathbf{e}_u(s_k)\cdot\mathbf{e}_v'(s_k) \tag{21}$$

where again the last equation follows from (8).

3.5 The Katsevich (K) scheme

Katsevich [11] developed this scheme also as a simpler alternative to the NHDLH scheme for the curved detector geometry and helical source curves. The scheme does contain a free parameter ε. Its general form reads

$$\begin{aligned} & g'(s_k, u_{i+\frac{1}{2}}) \simeq g'_{\mathrm{K}}(s_k, u_{i+\frac{1}{2}}) \\ &= \varepsilon \frac{(g_{k+1,i+1} - g_{k,i+1}) + (g_{k,i} - g_{k-1,i})}{2\Delta s} + (1-\varepsilon)\frac{(g_{k+1,i} - g_{k,i}) + (g_{k,i+1} - g_{k-1,i+1})}{2\Delta s} \\ &\quad + \frac{\partial u}{\partial s}(s_k, \theta(s_k, u_{i+\frac{1}{2}}))\, \frac{g_{k,i+1} - g_{k,i}}{\Delta u} \end{aligned} \tag{22}$$

with $\frac{\partial u}{\partial s}(s_k, \theta(s_k, u_{i+\frac{1}{2}}))$ given by (21). Compared to the FHS scheme the free parameter ε gives the K scheme added flexibility in discretizing the derivative with respect to s. (Here ε corresponds to $r\Delta s$ in [11].) Katsevich found that $\varepsilon = 0$ gave the highest resolution at the cost of some undershooting, and that $\varepsilon = 1/2$ provides a good tradeoff between resolution and noise stability. For this value of ε (i.e., $\varepsilon = 1/2$) the K scheme simplifies to the FHS scheme.

4 Summary of results and discussion

In this section we present and discuss the major results of the analysis of the schemes for a circular source curve $\mathbf{y}(s) = R(\cos s, \sin s)$ with curved detector geometry such that the center of the detector array is collinear with the origin and the source position $\mathbf{y}(s)$. The derivations are presented in the next section. In this geometry the variable u denotes the fan angle. In keeping with standard notation we rename u into α when working with this geometry.

The variables s and α are discretized with stepsizes Δs and $\Delta\alpha$, respectively. The two stepsizes are chosen proportional to each other, usually with Δs being significantly larger than $\Delta\alpha$. Optimal sampling conditions for this geometry are well known; see, e.g., [2, 13] and the references cited there. This theory relates the two stepsizes by $\Delta s \simeq (1+R)\Delta\alpha$. In practice Δs can often be chosen even larger. Similar sampling conditions hold true for the flat detector geometry [6].

4.1 A common framework

We note that the schemes are either based on directly discretizing (1) or using the chain rule equation (7). For a comparison of all schemes it is helpful to rewrite the direct scheme and the NHDLH scheme such that they appear as schemes based on (7). For the detector geometry under consideration equation (9) simplifies to $\frac{\partial\alpha(s,\theta)}{\partial s} = 1$, so that (7) reads $g'(s,\alpha) = g_s(s,\alpha) + g_\alpha(s,\alpha)$. For the direct scheme we obtain in this case $\tilde{u}_0 = \alpha_i - \Delta s/2$ and $\tilde{u}_1 = \alpha_i + \Delta s/2$ so that the direct scheme reads

$$g'_{\mathrm{dir}}(s_{k+\frac{1}{2}}, \alpha_i) = \frac{\mathscr{I}g(s_{k+1}, \alpha_i + \frac{1}{2}\Delta s) - \mathscr{I}g(s_k, \alpha_i - \frac{1}{2}\Delta s)}{\Delta s}.$$

Now observe that

$$\begin{aligned}
2\,[\mathscr{I}g(s_{k+1},\alpha_i+\Delta s/2)-\mathscr{I}g(s_k,\alpha_i-\Delta s/2)\,] \\
&= \mathscr{I}g(s_{k+1},\alpha_i+\Delta s/2)-\mathscr{I}g(s_{k+1},\alpha_i-\Delta s/2) \\
&\quad +\mathscr{I}g(s_{k+1},\alpha_i-\Delta s/2)-\mathscr{I}g(s_k,\alpha_i-\Delta s/2) \\
&\quad +\mathscr{I}g(s_{k+1},\alpha_i+\Delta s/2)-\mathscr{I}g(s_k,\alpha_i+\Delta s/2) \\
&\quad +\mathscr{I}g(s_k,\alpha_i+\Delta s/2)-\mathscr{I}g(s_k,\alpha_i-\Delta s/2)
\end{aligned}$$

and therefore the direct scheme can viewed as an approximation for g_s+g_α by

$$\begin{aligned}
g_s(s_{k+1/2},\alpha_i) &\approx \frac{1}{2\Delta s}[\mathscr{I}g(s_{k+1},\alpha_i+\Delta s/2)-\mathscr{I}g(s_k,\alpha_i+\Delta s/2) \\
&\quad +\mathscr{I}g(s_{k+1},\alpha_i-\Delta s/2)-\mathscr{I}g(s_k,\alpha_i-\Delta s/2)] \\
g_\alpha(s_{k+1/2},\alpha_i) &\approx \frac{1}{2\Delta s}[\mathscr{I}g(s_{k+1},\alpha_i+\Delta s/2)-\mathscr{I}g(s_{k+1},\alpha_i-\Delta s/2) \\
&\quad +\mathscr{I}g(s_k,\alpha_i+\Delta s/2)-\mathscr{I}g(s_k,\alpha_i-\Delta s/2)].
\end{aligned} \tag{23}$$

We see that the partial derivative with respect to α is discretized with step size $\Delta s \gg \Delta\alpha$ instead of $\Delta\alpha$. This indicates that this natural choice for the discretization may be the least effective method discussed here because of the step size Δs used for approximating the partial derivative with respect to α is too large. The error analysis given below will confirm this finding.

Rewriting the NHDLH scheme is less straightforward. For the case that $\alpha_i \le \mu_\pm, \nu_\pm \le \alpha_{i+1}$, equation (54), derived in section 5 below, gives

$$\begin{aligned}
g'_{\mathrm{NHDLH}}(s_k,\alpha_{i+\frac{1}{2}}) &= (1-c)\,\frac{g_{k+1,i}-g_{k-1,i}}{2\Delta s} \;+\; c\,\frac{g_{k+1,i+1}-g_{k-1,i+1}}{2\Delta s} \\
&\quad +\left(\frac{\mu_+-\mu_-}{2\Delta s}\right)\frac{g_{k-1,i+1}-g_{k-1,i}}{\Delta\alpha} \;+\; (1-\varepsilon)\left(\frac{\nu_+-\nu_-}{2\varepsilon\Delta s}\right)\frac{g_{k,i+1}-g_{k,i}}{\Delta\alpha}
\end{aligned}$$

with $c=\frac{\mu_+-\alpha_i}{\Delta\alpha}$. It is apparent that the approximation of g_s will mostly come from the first two terms and the approximation of g_α from the last two terms.

4.2 Leading error terms

The leading error terms for the schemes that will be derived in the next section are as follows.

$$\text{FHS:}\quad (\Delta\alpha)^2\left(\frac{g_{\alpha\alpha\alpha}}{24}+\frac{g_{s\alpha\alpha}}{8}\right)+(\Delta s)^2\,\frac{g_{sss}}{6} \tag{24}$$

$$\text{NPH:}\quad (\Delta\alpha)^2\left(\frac{g_{\alpha\alpha\alpha}}{24}+\frac{g_{s\alpha\alpha}}{8}\right)+(\Delta s)^2\left(\frac{1}{4}\frac{g_{sss}}{6}+\frac{g_{ss\alpha}}{8}\right) \tag{25}$$

$$\text{K:}\quad (\Delta\alpha)^2\left(\frac{g_{\alpha\alpha\alpha}}{24}+\frac{g_{s\alpha\alpha}}{8}\right)+(\Delta s)^2\,\frac{g_{sss}}{6}+\Delta s\Delta\alpha(2\varepsilon-1)\frac{g_{ss\alpha}}{4} \tag{26}$$

$$\begin{aligned}\text{NHDLH:}\quad &(\Delta\alpha)^2\left(\frac{g_{\alpha\alpha\alpha}}{24}+\frac{g_{s\alpha\alpha}}{8}\right)+(\Delta s)^2\,\frac{g_{sss}}{6}\\ &+(\Delta s)^2\left(\left(d(\varepsilon,\alpha)+\frac{\varepsilon^2}{2}(\varepsilon-1)\right)g_\alpha-\frac{(\varepsilon-1)^2}{2}\tan\alpha\,g_{s\alpha}+\frac{\varepsilon}{2}g_{ss\alpha}\right)\\ &d(\varepsilon,\alpha)=O((1-\varepsilon)^2\sec^2\alpha),\ \alpha=\alpha_{i+\frac{1}{2}}\end{aligned} \tag{27}$$

$$\begin{aligned}\textit{Direct}:\quad &(\Delta\alpha)^2\,\frac{c}{2}(1-c)\left(g_{s\alpha\alpha}+\left(1+\frac{2(1-2c)}{3}\frac{\Delta\alpha}{\Delta s}\right)g_{\alpha\alpha\alpha}\right)\\ &+(\Delta s)^2\left(\frac{g_{\alpha\alpha\alpha}}{24}+\frac{g_{s\alpha\alpha}}{8}+\frac{g_{ss\alpha}}{8}+\frac{g_{sss}}{24}\right)\\ &c=(\alpha_i+\Delta s/2-\alpha_{i+J})/\Delta\alpha,\ \text{with } J \text{ such that } \alpha_{i+J}\le\alpha_i+\Delta s/2<\alpha_{i+J+1}\end{aligned} \tag{28}$$

In each expression the partial derivatives of g are evaluated at the point where the respective scheme approximates the view dependent derivative. The expressions for the NHDLH schemes are derived under the assumption that $\alpha_i\le\mu_\pm,\nu_\pm\le\alpha_{i+1}$ which promises the highest resolution but requires ε and Δs to be sufficiently small, as will be further explained in section 5 below.

The leading error terms of the FHS scheme are shared by the K and NHDLH schemes which have also additional terms. However, this by itself does not imply that the FHS scheme must always be more accurate since there is the possibility of some cancellation when the error terms are added together, as well as during the subsequent filtering and back projection steps of the image reconstruction.

Further aspects will now be discussed in the context of numerical experiments.

4.3 Numerical experiments and discussion

For each of the following experiments we use a reconstruction algorithm based on the inversion formula (2) with numerical implementation as described in [4, §7] and choice of $I_\pi(\mathbf{x})$ corresponding to orthogonal-long π-lines, also described in [4]. Unless specified otherwise, the source radius R equals 3 and the reconstructions are computed inside the unit circle on a grid of 256 by 256 pixels.

The mathematical phantoms are linear combinations of functions of the form

$$f(\mathbf{x})=b_m(T(\mathbf{x}-\mathbf{x}_0)) \tag{29}$$

with

$$b_m(\mathbf{x})=\left(1-|\mathbf{x}|^2\right)_+^m=\begin{cases}\left(1-|\mathbf{x}|^2\right)^m & \text{if } 1-|\mathbf{x}|^2>0\\ 0 & \text{if } 1-|\mathbf{x}|^2\le 0\end{cases}. \tag{30}$$

P	direct scheme error	γ	NPH error	γ
128	0.13237		0.010073	
256	0.035998	1.8786	0.0025395	1.9879
512	0.0092159	1.9657	0.00063654	1.9962
1024	0.0023187	1.9908	0.00015921	1.9993
2048	0.00058064	1.9976	3.9792×10^{-5}	2.0004
4096	0.00014522	1.9994	9.9485×10^{-6}	1.9999

Table 1 Convergence study for the direct and NPH schemes for the phantom (29) with parameters $m=3$, $\mathbf{x}_0=(0.2,0.3), u=.35, v=.25, \psi=25\pi/180$, $\Delta s=2\pi/P$ and $\Delta\alpha=4\arcsin(1/R)/P$ where $R=3$ is the radius of the source circle.

P	FHS error	γ	NHDLH error	γ	K error	γ
128	0.0055806		0.0064163		0.0042778	
256	0.0013914	2.0039	0.0016050	1.9991	0.0010613	2.0111
512	0.00034813	1.9988	0.00040178	1.9981	0.00026550	1.9990
1024	8.6974×10^{-5}	2.0010	0.00010041	2.0005	6.6293×10^{-5}	2.0018
2048	2.1713×10^{-5}	2.0020	2.5077×10^{-5}	2.0015	1.6532×10^{-5}	2.0036
4096	5.4282×10^{-6}	2.0000	6.2695×10^{-6}	2.0000	4.1330×10^{-6}	2.0000

Table 2 Convergence study for difference schemes FHS, NHDLH with $\varepsilon=\Delta\alpha/(4\Delta s)$, and K with $\varepsilon=0$ for the phantom (29) with the same parameters as in Table 1.

The matrix

$$T=\begin{bmatrix}\cos(\psi)/u & \sin(\psi)/u\\ -\sin(\psi)/v & \cos(\psi)/v\end{bmatrix}$$

allows for dilation and rotation so that the support of f is an elliptical disk with center $\mathbf{x}_0$ and half axes u and v. The parameter m controls the smoothness of the function. For $m=0$ one obtains the characteristic function of the support. The well known Shepp-Logan phantom can be expressed as a linear combination of such functions.

The relative l_2 error of the reconstructions is calculated by

$$\left(\frac{\sum_{i,j}(\bar{f}(\mathbf{x}_{i,j})-f(\mathbf{x}_{i,j}))^2}{\sum_{i,j}f(\mathbf{x}_{i,j})^2}\right)^{1/2}, \tag{31}$$

where $\bar{f}$ is the numerical reconstruction and f is the exact function.

1. **Order of convergence.** The first experiment, presented in Tables 1 and 2, is a convergence study. It also provides an indication of the relative accuracy of the schemes when reconstructing a sufficiently smooth function, in this case f as in (29) with $m=3$. We use $P=2^j$ source positions so that $\Delta s=2\pi/P$ and choose $\Delta\alpha$ proportional to Δs in such a way that the condition $\Delta s\geq(1+R)\Delta\alpha$ is satisfied, i.e., $R=3$ and $\Delta s/\Delta\alpha=\pi/(2\arcsin(1/R))\simeq 4.62$. In these reconstructions the convolutions are computed on a denser grid with spacing $\Delta\alpha/8$ in order to suppress the errors from the interpolation in the backprojection step of the algorithm.
   The leading error terms (24)–(28) give second order accuracy for all schemes. The discretizations used for the two integrations in (2) also have second order accuracy, so that the reconstruction error (31) can be expected to decay as $O(P^{-\gamma})$ with $\gamma=2$. The tables show numerically computed values of γ which are indeed very close to 2, confirming the expectation from the leading error terms. This rate of convergence is the same as that for the parallel-beam filtered back projection algorithm with the Shepp-Logan convolution kernel [19, Example 5.1].

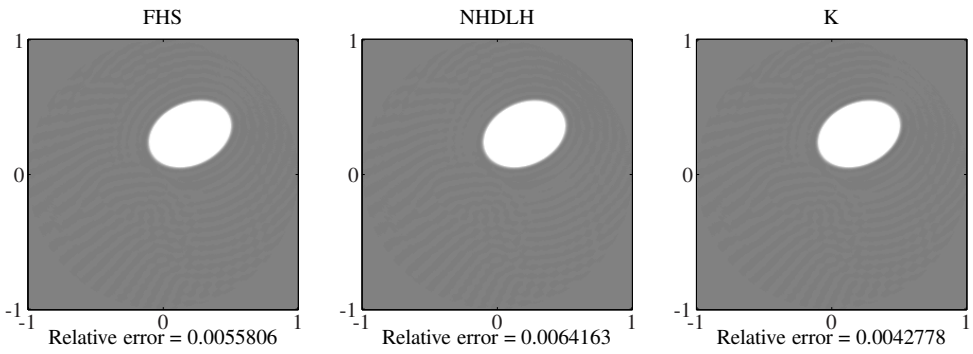

Fig. 3 Reconstructions of the smooth function (29) with parameters as in the first row of Table 2.

For the FHS, NHDLH and K schemes the errors are quite close to each other, with the K scheme (with $\varepsilon = 0$) having the lowest error. The errors for the NPH scheme are somewhat larger while the errors for the direct scheme are an order of magnitude larger. When inspecting the error terms (28) for the direct scheme one finds that the terms $(g_{\alpha\alpha\alpha}/24 + g_{s\alpha\alpha}/8)$ are multiplied by $(\Delta s)^2$ instead of $(\Delta\alpha)^2$ as for the other schemes. This is a consequence of the approximation for g_α in (23) being computed with a step size of Δs instead of $\Delta\alpha$. Since $(\Delta s)^2$ is much larger than $(\Delta\alpha)^2$ this confirms the numerical experience that the direct scheme is significantly less accurate.
For the FHS, NHDLH, and K schemes we also present the images of the reconstructions for the case $P = 128$ in Figure 3.

2. **Non-isotropy of the NPH scheme.** When comparing the error terms (24), (25) for the NPH and FHS schemes one sees that the main difference appears to be the additional term $(\Delta s)^2 g_{ss\alpha}/8$, and the question arises if this term is mainly responsible for the non-isotropic resolution of the NPH scheme. The following numerical experiment indicates that this seems indeed to be the case.
The top left image in Figure 4 shows the original function (29) and the top right image its reconstruction using the NPH scheme. The nonisotropy is clearly visible. The bottom left image shows a reconstruction of the error term $(\Delta s)^2 \frac{g_{ss\alpha}}{8}$ and the bottom right shows difference between the top right and bottom left images, that is, the reconstruction using the NPH scheme but with the error term subtracted. The non-isotropy is less pronounced. It is intriguing that both the NHDLH and the K scheme also have an error term proportional to $g_{ss\alpha}$ but are not known to show the non-isotropic resolution of the NPH scheme. In the case of the NHDLH scheme the choice $\varepsilon = 1/4$ would make the term $\frac{\varepsilon}{2} g_{ss\alpha}$ equal to the corresponding term for the NPH scheme and for this choice of ε one indeed obtains a very similar result to that shown in the top right of Figure 4 for the NPH scheme. However, $\varepsilon = 1/4$ or even larger is simply not a good choice in this case. It is too large for our assumption that $\alpha_i \le \mu_\pm, \nu_\pm \le \alpha_{i+1}$ to hold and the user is free to choose a much smaller value which makes the error term insignificant and gives good results. Similar findings hold true for the K scheme. On the one hand, for the K scheme with $0 \le \varepsilon \le 1$ and $\Delta s \gg \Delta\alpha$ the factor $\Delta s \Delta\alpha(2\varepsilon - 1)/4$ multiplying $g_{ss\alpha}$ is significantly smaller than the corresponding factor $(\Delta s)^2/8$ for the NPH scheme, so this error term is unlikely to have an observable effect . On the other hand, if ε in the K scheme is chosen excessively large such that $\Delta s \Delta\alpha(2\varepsilon - 1)/4 \simeq (\Delta s)^2/8$, then non-isotropy can be observed for the K scheme as well.

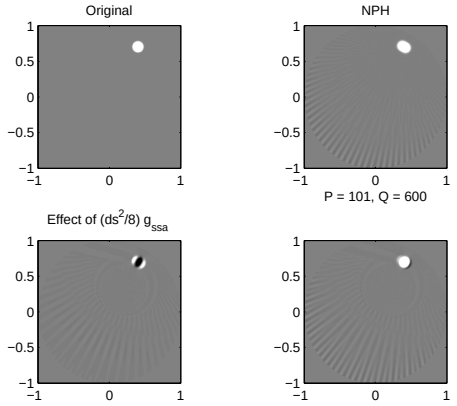

Fig. 4 Non-isotropy of the NPH scheme. Top left: Original function (29) with $m = 3$, $\psi = 0$, $u = v = 0.1$, $\mathbf{x}_0 = (0.4, 0.7)$. Top right: Reconstruction using the NPH scheme. Bottom left: Reconstruction of the error term $(\Delta s)^2 \frac{g_{ss\alpha}}{8}$. Bottom right: Reconstruction using NPH scheme but with error term subtracted. All reconstructions performed with $\Delta s = 2\pi/101$ and $\Delta\alpha = \pi/600$.

3. **Additional error terms of the NHDLH scheme.** The NHDLH scheme has additional error terms that depend on $\tan(\alpha)$ and $\sec^2(\alpha)$ which can become large for $|\alpha|$ very close to $\pi/2$. This case can occur when the source radius R is very close to 1, so that rays with fan angle α close to $\pi/2$ pass through the object. However, in our experiments for such cases we did not find any significant additional errors caused by these terms.
4. **Flat detectors and elliptical source curves.** The theory presented here does not cover flat detectors or elliptical source curves. It appears that the case of flat detectors and circular source curve could be worked out with the methods presented here, while the analysis for an elliptical source curve, in particular for the NHDLH scheme, is more complex. We did, however, perform preliminary numerical experiments for flat detectors and for an elliptical source curve. For a circular source curve the results for flat detectors mirrored those for curved detectors. For an elliptical source curve the results for the FHS and K schemes turned out to be dependent on the particular detector alignment. The errors and visual images for the FHS, NHDLH, and K schemes remained very close to each other when the vector $\mathbf{e}_u(s)$ defined at the beginning of section 2 was chosen to be perpendicular to the source position vector $\mathbf{y}(s)$. Figure 5 shows reconstructions of the Shepp-Logan phantom for flat detectors with this alignment. The three schemes lead to very comparable images and errors. The corresponding results for curved detectors are very similar and therefore not shown here. On the other hand, in the case of an elliptical source curve and flat detectors aligned such that $\mathbf{e}_u(s)$ is parallel to $\frac{d}{ds}\mathbf{y}(s)$ the FHS and K schemes produced significant artifacts while our experiments confirmed the findings of [17] that the NHDLH scheme continues to perform very well in this situation. A theoretical explanation for this difference in performance will be subject of our future research.

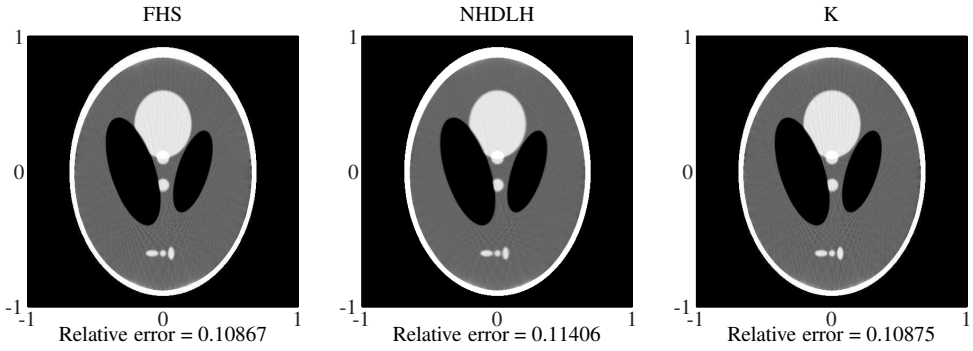

Fig. 5 Reconstructions of the Shepp-Logan phantom with a flat detector array for the FHS, NHDLH (with $\varepsilon = 0.125$) and K (with $\varepsilon = 0$) schemes. The source curve is the ellipse $\mathbf{y}(s) = (3.6\cos(s),\ 2.4\sin(s)),\ s \in [0, 2\pi]$. Detectors are aligned such that $\mathbf{e}_u(s)$ is perpendicular to $\mathbf{y}(s)$. The reconstruction grid has 512×512 pixels, $\Delta s = 2\pi/501$, $\Delta u = 0.01$, $D = 3$. The gray scale is compressed on the interval $[1.012, 1.032]$.

5 Error analysis of the schemes for the curved detector geometry and circular source curve

We consider a circular source curve $\mathbf{y}(s) = R(\cos s, \sin s)$ with curved detector geometry aligned such that the center of the detector array is collinear with the origin and the source position $\mathbf{y}(s)$. This gives

$$\mathbf{e}_v(s) = -\mathbf{y}(s)/|\mathbf{y}(s)| = -(\cos s, \sin s), \quad \mathbf{e}_u(s) = (-\sin s, \cos s).$$

As mentioned above, we rename u into α when working with this geometry. Now equation (9) simplifies to

$$\frac{\partial \alpha(s,\theta)}{\partial s} = 1, \tag{32}$$

so that (7) reads

$$\frac{d}{dq}\mathscr{D}f(\mathbf{y}(q),\theta)\bigg|_{q=s} = \frac{\partial g}{\partial s}(s,\alpha(s,\theta)) + \frac{\partial g}{\partial \alpha}(s,\alpha(s,\theta)).$$

or equivalently,

$$g'(s,\alpha) = g_s(s,\alpha) + g_\alpha(s,\alpha).$$

Equation (5) reads

$$\theta(s,\alpha) = \sin\alpha\, \mathbf{e}_u(s) + \cos\alpha\, \mathbf{e}_v(s)$$

which implies the two relations

$$\begin{aligned} \alpha(s,\theta) &= \arcsin(\theta \cdot \mathbf{e}_u(s)) \\ &= \arctan\left(\frac{\theta \cdot \mathbf{e}_u(s)}{\theta \cdot \mathbf{e}_v(s)}\right). \end{aligned} \tag{33}$$

5.1 Error analysis for the direct scheme

For this geometry (13) reads $\tilde{u}_0 = \alpha_i - \frac{1}{2}\Delta s$, $\tilde{u}_1 = \alpha_i + \frac{1}{2}\Delta s$, hence

$$g'_{\mathrm{dir}}(s_{k+\frac{1}{2}}, \alpha_i) = \frac{\mathscr{I}g(s_{k+1}, \alpha_i + \frac{1}{2}\Delta s) - \mathscr{I}g(s_k, \alpha_i - \frac{1}{2}\Delta s)}{\Delta s}$$

Proposition 1 *(Error for the direct scheme) Let $g(s,\alpha)$ be C^4 on $\mathbb{R}\times[-\pi,\pi)$, $s_k = k\Delta s$ and $\alpha_i = i\Delta\alpha$. Then*

$$\begin{aligned} g'_{dir}(s_{k+\frac{1}{2}}, \alpha_i) - g'(s_{k+\frac{1}{2}}, \alpha_i) = (\Delta\alpha)^2 \frac{c}{2}(1-c)\left(g_{s\alpha\alpha} + \left(1 + \frac{2(1-2c)}{3}\frac{\Delta\alpha}{\Delta s}\right) g_{\alpha\alpha\alpha}\right) \\ + (\Delta s)^2 \left(\frac{g_{sss}}{24} + \frac{g_{ss\alpha}}{8} + \frac{g_{s\alpha\alpha}}{8} + \frac{g_{\alpha\alpha\alpha}}{24}\right) + O(\Delta s^3 + \Delta\alpha^2\Delta s) \end{aligned} \tag{34}$$

where $c = (\alpha_i + \Delta s/2 - \alpha_{i+J})/\Delta\alpha$, J is such that $\alpha_{i+J} \le \alpha_i + \Delta s/2 < \alpha_{i+J+1}$, and the partial derivatives of g in (34) are evaluated at the point $(s_{k+\frac{1}{2}}, \alpha_i)$.

In the proof of Proposition 1 we will use the following observation about the error of linear interpolation.

Lemma 1 *Let $f \in C^4(\mathbb{R})$, $\alpha_i = i\Delta\alpha$, $\alpha_i < t < \alpha_{i+1}$ and*

$$\mathscr{I}f(t) = (1-c)f(\alpha_i) + cf(\alpha_{i+1}) \text{ with } c = (t-\alpha_i)/\Delta\alpha. \tag{35}$$

Then

$$\mathscr{I}f(t) - f(t) = \frac{c(1-c)\Delta\alpha^2}{2} f''(t) + \frac{c(1-c)(1-2c)\Delta\alpha^3}{6} f'''(t) + O(\Delta\alpha^4).$$

Proof The assertion follows directly from replacing $f(\alpha_i)$ and $f(\alpha_{i+1})$ in (35) by their Taylor expansions about t.

Proof (Proposition 1 for the direct scheme) We write the error as the sum of a discretization error and an interpolation error.

$$\begin{aligned} & g'_{\mathrm{dir}}(s_{k+\frac{1}{2}}, \alpha_i) - g'(s_{k+\frac{1}{2}}, \alpha_i) \\ &= \left(\frac{g(s_{k+1}, \alpha_i + \Delta s/2) - g(s_k, \alpha_i - \Delta s/2)}{\Delta s} - g'(s_{k+\frac{1}{2}}, \alpha_i)\right) \\ &\quad + \frac{(\mathscr{I}g - g)(s_{k+1}, \alpha_i + \Delta s/2) - (\mathscr{I}g - g)(s_k, \alpha_i - \Delta s/2)}{\Delta s} \end{aligned} \tag{36}$$

Let $\alpha_i = i\Delta\alpha$ and $\alpha_{i+J} \le \alpha_i + \Delta s/2 < \alpha_{i+J+1}$. Then $\alpha_i + \Delta s/2 = (1-c)\alpha_{i+J} + c\alpha_{i+J+1}$ with $c = (\alpha_i + \Delta s/2 - \alpha_{i+J})/\Delta\alpha$, and $\mathscr{I}g(s_{k+1}, \alpha_i + \Delta s/2) = (1-c)g(s_{k+1}, \alpha_{i+J}) + cg(s_{k+1}, \alpha_{i+J+1})$. Likewise $\alpha_i - \Delta s/2 = c\,\alpha_{i-J-1} + (1-c)\alpha_{i-J}$ so that $\mathscr{I}g(s_k, \alpha_i - \Delta s/2) = (1-\tilde{c})g(s_k, \alpha_{i-J-1}) + \tilde{c}g(s_k, \alpha_{i-J})$ with $\tilde{c} = 1-c$. Note that

$$\tilde{c}(1-\tilde{c}) = c(1-c) \text{ while } \tilde{c}(1-\tilde{c})(1-2\tilde{c}) = -c(1-c)(1-2c).$$

It then follows from Lemma 1 that

$$\begin{aligned}
&(\mathscr{I}g-g)(s_{k+1},\alpha_i+\Delta s/2)-(\mathscr{I}g-g)(s_k,\alpha_i-\Delta s/2)\\
&=\frac{c(1-c)}{2}\Delta\alpha^2\left(g_{\alpha\alpha}(s_{k+1},\alpha_i+\Delta s/2)-g_{\alpha\alpha}(s_k,\alpha_i-\Delta s/2)\right)\\
&\quad+\frac{c(1-c)(1-2c)}{6}\Delta\alpha^3\left(g_{\alpha\alpha\alpha}(s_{k+1},\alpha_i+\Delta s/2)+g_{\alpha\alpha\alpha}(s_k,\alpha_i-\Delta s/2)\right)+O(\Delta\alpha^4)
\end{aligned}$$

The 2D Taylor expansions of $g_{\alpha\alpha}(s_{k+1},\alpha_i+\Delta s/2)$ and $g_{\alpha\alpha}(s_k,\alpha_i-\Delta s/2)$ about the point $(s_{k+\frac{1}{2}},\alpha_i)$ yield

$$\begin{aligned}
&g_{\alpha\alpha}(s_{k+1},\alpha_i+\Delta s/2)-g_{\alpha\alpha}(s_k,\alpha_i-\Delta s/2)\\
&\quad=\Delta s\,g_{\alpha\alpha\alpha}(s_{k+1/2},\alpha_i)+\Delta s\,g_{s\alpha\alpha}(s_{k+1/2},\alpha_i)+O(\Delta s^3).
\end{aligned}$$

Similarly one obtains for the third order error terms

$$g_{\alpha\alpha\alpha}(s_{k+1},\alpha_i+\Delta s/2)+g_{\alpha\alpha\alpha}(s_k,\alpha_i-\Delta s/2)\;=\;2g_{\alpha\alpha\alpha}(s_{k+1/2},\alpha_i)+O(\Delta s^2).$$

Therefore the interpolation error satisfies

$$\begin{aligned}
&\frac{1}{\Delta s}\left[(\mathscr{I}g-g)(s_{k+1},\alpha_i+\Delta s/2)-(\mathscr{I}g-g)(s_k,\alpha_i-\Delta s/2)\right]\\
&=\frac{c}{2}(1-c)\Delta\alpha^2\left(g_{s\alpha\alpha}(s_{k+1/2},\alpha_i)+\left(1+\frac{2(1-2c)\Delta\alpha}{3\Delta s}\right)g_{\alpha\alpha\alpha}(s_{k+1/2},\alpha_i)\right)\\
&\quad+O(\Delta\alpha^2\Delta s)
\end{aligned}\tag{37}$$

where we have used that $O\left(\Delta\alpha^2\left(\Delta s^2+\Delta s\Delta\alpha+\frac{\Delta\alpha^2}{\Delta s}\right)\right)=O\left(\Delta\alpha^2\Delta s\left(\Delta s+\Delta\alpha+\left(\frac{\Delta\alpha}{\Delta s}\right)^2\right)\right)=O(\Delta\alpha^2\Delta s)$ since we assume that $\Delta\alpha<\Delta s$ and $\Delta\alpha/\Delta s$ is bounded away from zero as Δs and $\Delta\alpha$ approach zero.

Recalling that $g'(s_{k+1/2},\alpha_i)=g_s(s_{k+\frac{1}{2}},\alpha_i)+g_\alpha(s_{k+\frac{1}{2}},\alpha_i)$, the expression for the discretization error follows directly from Taylor expansions of $g(s_{k+1},\alpha_i+\Delta s/2)$ and $g(s_k,\alpha_i-\Delta s/2)$ about the point $(s_{k+\frac{1}{2}},\alpha_i)$. This gives

$$\begin{aligned}
&\frac{g(s_{k+1},\alpha_i+\Delta s/2)-g(s_k,\alpha_i-\Delta s/2)}{\Delta s}-g'(s_{k+\frac{1}{2}},\alpha_i)\\
&=\frac{\Delta s^2}{24}\left(g_{sss}+3g_{ss\alpha}+3g_{s\alpha\alpha}+g_{\alpha\alpha\alpha}\right)+O(\Delta s^3)
\end{aligned}\tag{38}$$

where the partial derivatives of g are evaluated at the point $(s_{k+\frac{1}{2}},\alpha_i)$. The Proposition now follows from inserting (37) and (38) into (36).

Because of (32) the NPH scheme reads in our current detector geometry as follows.

$$\begin{aligned}
&g'_{\mathrm{NPH}}(s_{k+\frac{1}{2}},\alpha_{i+\frac{1}{2}})\\
&=\frac{\left[(g_{k+1,i+1}-g_{k,i+1})\;+\;(g_{k+1,i}-g_{k,i})\right]}{2\Delta s}\;+\;\frac{\left[(g_{k+1,i+1}-g_{k+1,i})+(g_{k,i+1}-g_{k,i})\right]}{2\Delta\alpha}
\end{aligned}$$

where the first term approximates $g_s(s_{k+\frac{1}{2}},\alpha_{i+\frac{1}{2}})$ and the second $g_\alpha(s_{k+\frac{1}{2}},\alpha_{i+\frac{1}{2}})$.

Proposition 2 *(Error for the NPH scheme) Let $g(s,\alpha)$ be C^4 on $\mathbb{R}\times[-\pi,\pi)$, $s_k = k\Delta s$ and $\alpha_i = i\Delta\alpha$. Then*

$$\begin{aligned} &g'_{NPH}(s_{k+\frac{1}{2}},\alpha_{i+\frac{1}{2}}) - g'(s_{k+\frac{1}{2}},\alpha_{i+\frac{1}{2}}) \\ &= \frac{\Delta\alpha^2}{24}(g_{\alpha\alpha\alpha}+3g_{s\alpha\alpha}) \;+\; \frac{\Delta s^2}{24}(g_{sss}+3g_{ss\alpha}) \;+\; O((\Delta s+\Delta\alpha)^3) \end{aligned} \tag{39}$$

where the partial derivatives of g are evaluated at the point $(s_{k+\frac{1}{2}},\alpha_{i+\frac{1}{2}})$.

The proof consists of a routine 2D Taylor expansion of g about the point $(s_{k+\frac{1}{2}},\alpha_{i+\frac{1}{2}})$.

Proposition 3 *(Error for the K scheme) Let $g(s,\alpha)$ be C^4 on $\mathbb{R}\times[-\pi,\pi)$, $s_k = k\Delta s$ and $\alpha_i = i\Delta\alpha$. Then*

$$\begin{aligned} &g_s(s_k,\alpha_{i+\frac{1}{2}}) \;-\; \left(\varepsilon\frac{(g_{k+1,i+1}-g_{k,i+1}) \;+\; (g_{k,i}-g_{k-1,i})}{2\Delta s} \;+\; (1-\varepsilon)\frac{(g_{k+1,i}-g_{k,i})+(g_{k,i+1}-g_{k-1,i+1})}{2\Delta s}\right) \\ &= -\left(\Delta\alpha^2\,\frac{g_{s\alpha\alpha}}{8} \;+\Delta s^2\,\frac{g_{sss}}{6} \;+\; \Delta s\Delta\alpha(2\varepsilon-1)\frac{g_{ss\alpha}}{4}\right) + O\left((\Delta s+\Delta\alpha)^3\right) \end{aligned}$$

and

$$g_\alpha(s_k,\alpha_{i+\frac{1}{2}}) \;-\; \frac{g_{k,i+1}-g_{k,i}}{\Delta\alpha} \;=\; -\frac{\Delta\alpha^2}{24}g_{\alpha\alpha\alpha} \;+\; O(\Delta\alpha^3).$$

Therefore

$$\begin{aligned} &g'_K(s_k,\alpha_{i+\frac{1}{2}}) - g'(s_k,\alpha_{i+\frac{1}{2}}) \\ &= \Delta\alpha^2\left(\frac{g_{\alpha\alpha\alpha}}{24} \;+\; \frac{g_{s\alpha\alpha}}{8}\right) \;+\; \Delta s^2\,\frac{g_{sss}}{6} \;+\; \Delta s\Delta\alpha(2\varepsilon-1)\frac{g_{ss\alpha}}{4} \\ &\quad + O\left((\Delta s+\Delta\alpha)^3\right), \end{aligned} \tag{40}$$

where the partial derivatives of g are evaluated at the point $(s_k,\alpha_{i+\frac{1}{2}})$.

As before the proposition follows from a 2D Taylor expansion of g, this time about the point $(s_k,\alpha_{i+\frac{1}{2}})$.

The corresponding result for the FHS scheme is obtained by setting $\varepsilon = 1/2$ in Proposition 3, since in this case the K-scheme equals the FHS scheme.

Corollary 1 *(Error for the FHS scheme) Let $g(s,\alpha)$ be C^4 on $\mathbb{R}\times[-\pi,\pi)$, $s_k = k\Delta s$ and $\alpha_i = i\Delta\alpha$. Then*

$$\begin{aligned} &g'_{FHS}(s_k,\alpha_{i+\frac{1}{2}}) - g'(s_k,\alpha_{i+\frac{1}{2}}) \\ &= \Delta\alpha^2\left(\frac{g_{\alpha\alpha\alpha}}{24} \;+\; \frac{g_{s\alpha\alpha}}{8}\right) \;+\; \Delta s^2\,\frac{g_{sss}}{6} \;+\; O\left((\Delta s+\Delta\alpha)^3\right), \end{aligned} \tag{41}$$

where the partial derivatives of g are evaluated at the point $(s_k,\alpha_{i+\frac{1}{2}})$.

Proposition 4 *(Error for the NHDLH scheme) Let $g(s,\alpha)$ be C^4 on $\mathbb{R}\times[-\pi,\pi)$, $s_k = k\Delta s$ and $\alpha_i = i\Delta\alpha$. If the $\mu_\pm$ and $\nu_\pm$ all lie in $[\alpha_i,\alpha_{i+1}]$, then*

$$\begin{aligned} &g'_{NHDLH}(s_k,\alpha_{i+\frac{1}{2}}) - g'(s_k,\alpha_{i+\frac{1}{2}}) \\ &= (\Delta s)^2\left(\left(d(\varepsilon,\alpha_{i+\frac{1}{2}}) + \frac{\varepsilon^2}{2}(\varepsilon-1)\right)g_\alpha \;-\; \frac{(\varepsilon-1)^2}{2}\tan\alpha_{i+\frac{1}{2}}\,g_{s\alpha} \;+\; \frac{\varepsilon}{2}g_{ss\alpha} \;+\; \frac{g_{sss}}{6}\right) \\ &\quad + (\Delta\alpha)^2\left(\frac{g_{\alpha\alpha\alpha}}{24}+\frac{g_{s\alpha\alpha}}{8}\right) \;+\; O\left((\Delta s+\Delta\alpha)^3\right) \end{aligned} \tag{42}$$

with

$$d(\varepsilon,\alpha) = -\frac{1}{4}(\varepsilon-1)^2\sec^2(\alpha)\left[(\varepsilon-1)\cos(2\alpha)+\varepsilon+1\right]. \tag{43}$$

The partial derivatives of g are evaluated at the point $(s_k, \alpha_{i+\frac{1}{2}})$.

Remark 1 Proposition 4 treats the situation of potentially highest resolution, where the $\nu_\pm$ and $\mu_\pm$ deviate by at most by $\Delta\alpha/2$ from $\alpha_{i+\frac{1}{2}}$ and thus the derivatives are discretized with smaller step sizes. While this assumption does require ε and Δs to be sufficiently small, this requirement is usually met with commonly used parameters. Sufficient conditions for this assumption to be valid are given in the proof of Proposition 4; see inequality (48) below.

Proof We first need analytical expressions for the $\nu_\pm$ and $\mu_\pm$. Let $\eta(t,s,\theta)$ denote the unit vector in the direction of the ray from $\mathbf{y}(t)$ to $\mathbf{b}(s,\theta) = \mathbf{y}(s) - (\mathbf{y}(s)\cdot\theta)\theta$, cf. section 3.3. Let $\tilde{\nu}(s,u,\alpha)$ be such that $\mathscr{D}f(y(s),\eta(s,s+u,\theta(s,\alpha)) = g(s,\tilde{\nu}(s,u,\alpha))$. Then $\nu_\pm = \tilde{\nu}(s_k,\pm\varepsilon\Delta s,\alpha_{i+\frac{1}{2}})$, cf. Figure 2. It follows from (33) that

$$\begin{aligned}\tilde{\nu}(s,u,\alpha) &= \arctan\left(\frac{\eta(s,s+u,\theta(s,\alpha))\cdot\mathbf{e}_u(s)}{\eta(s,s+u,\theta(s,\alpha))\cdot\mathbf{e}_v(s)}\right)\\ &= \arctan\left(\frac{2\cos(\alpha)\sin(\alpha+u))}{2-\cos(u)+\cos(2\alpha+u)}\right)\\ &= \nu(u,\alpha)\end{aligned} \tag{44}$$

A Taylor expansion with respect to u about $u=0$ yields

$$\nu(u,\alpha) = \alpha + u - \frac{u^2}{2}\tan\alpha - \frac{u^3}{2} + O(u^4) \tag{45}$$

Similarly, let $\tilde{\mu}(s,u,\alpha,\varepsilon)$ be such that $\mathscr{D}f(y(s+u),\eta(s+u,s+\varepsilon u,\theta(s,\alpha)) = g(s+u,\tilde{\mu}(s,u,\alpha,\varepsilon))$. Then $\mu_\pm = \tilde{\mu}(s_k,\pm\Delta s,\alpha_{i+\frac{1}{2}},\varepsilon)$ and

$$\begin{aligned}\tilde{\mu}(s,u,\alpha,\varepsilon) &= \arctan\left(\frac{\eta(s+u,s+\varepsilon u,\theta(s,\alpha))\cdot\mathbf{e}_u(s+u)}{\eta(s+u,s+\varepsilon u,\theta(s,\alpha))\cdot\mathbf{e}_v(s+u)}\right)\\ &= \arctan\left(\frac{2\cos(\alpha+u)\sin(\alpha+\varepsilon u)}{\cos(2\alpha+u+\varepsilon u)-\cos(u-\varepsilon u)+2}\right)\\ &= \mu(u,\alpha,\varepsilon)\end{aligned} \tag{46}$$

The Taylor expansion of $\mu(u,\alpha,\varepsilon)$ with respect to u about $u=0$ gives

$$\mu(u,\alpha,\varepsilon) = \alpha + \varepsilon u - \frac{(\varepsilon-1)^2}{2}\tan(\alpha)\,u^2 + d(\varepsilon,\alpha)\,u^3 + O(u^4) \tag{47}$$

with $d(\varepsilon,\alpha)$ as in (43).

The Taylor expansions allow to examine further the validity of the assumption that the $\nu_\pm$ and $\mu_\pm$ lie in $[\alpha_i,\alpha_{i+1}]$. For example, since $\nu_\pm = \nu(\pm\varepsilon\Delta s,\alpha_{i+\frac{1}{2}})$, one has

$$|\nu_\pm - \alpha_{i+\frac{1}{2}}| = \varepsilon\Delta s + \frac{(\varepsilon\Delta s)^2}{2}\frac{\partial^2\nu}{\partial u^2}(t,\alpha_{i+\frac{1}{2}})$$

for some $t\in[0,\varepsilon\Delta s]$. Let $M_\nu = \max_{0\le t\le\varepsilon\Delta s}\left|\frac{\partial^2\nu}{\partial u^2}(t,\alpha_{i+\frac{1}{2}})\right|$. Then $|\nu_\pm - \alpha_{i+\frac{1}{2}}| \le \Delta\alpha/2$ if $2\varepsilon\Delta s + (\varepsilon\Delta s)^2 M_\nu \le \Delta\alpha$. Similarly one obtains that $|\mu_\pm - \alpha_{i+\frac{1}{2}}| \le \Delta\alpha/2$ if $2\varepsilon\Delta s +$

$(\Delta s)^2 M_\mu \le \Delta\alpha$ with $M_\mu = \max_{0\le t\le \Delta s}\left|\frac{\partial^2 \mu}{\partial u^2}(t,\alpha_{i+\frac{1}{2}},\varepsilon)\right|$. The two conditions can be combined into one by using $(\varepsilon\Delta s)^2 \le (\Delta s)^2$ and defining $M = \max(M_\mu, M_\nu)$ to yield $2\varepsilon\Delta s + (\Delta s)^2 M \le \Delta\alpha$, or equivalently

$$0 \;<\; \varepsilon \;\le\; \frac{\Delta\alpha - \Delta s^2 M}{2\Delta s}. \tag{48}$$

By subtracting and adding back the term $\mathscr{I}g(s_{k-1},\mu_+)$ in the numerator of the first fraction in (19) the NHDLH scheme can be written equivalently as

$$\begin{aligned} g'_{\mathrm{NHDLH}}(s_k,\alpha_{i+\frac{1}{2}}) = {} & \frac{\mathscr{I}g(s_{k+1},\mu_+) - \mathscr{I}g(s_{k-1},\mu_+)}{2\Delta s} + \frac{\mathscr{I}g(s_{k-1},\mu_+) - \mathscr{I}g(s_{k-1},\mu_-)}{2\Delta s} \\ & + (1-\varepsilon)\frac{\mathscr{I}g(s_k,\nu_+) - \mathscr{I}g(s_k,\nu_-)}{2\varepsilon\Delta s} \end{aligned} \tag{49}$$

We next address the effect of the linear interpolation. Since $\alpha_i < \mu_\pm < \alpha_{i+1}$ it follows that

$$\begin{aligned} \frac{\mathscr{I}g(s_{k+1},\mu_+) - \mathscr{I}g(s_{k-1},\mu_+)}{2\Delta s} &= \frac{1}{2\Delta s}[(1-c)g(s_{k+1},\alpha_i) + cg(s_{k+1},\alpha_{i+1}) \\ &\quad -(1-c)g(s_{k-1},\alpha_i) - cg(s_{k-1},\alpha_{i+1})] \\ &= (1-c)\frac{g(s_{k+1},\alpha_i) - g(s_{k-1},\alpha_i)}{2\Delta s} \\ &\quad + c\frac{g(s_{k+1},\alpha_{i+1}) - g(s_{k-1},\alpha_{i+1})}{2\Delta s} \end{aligned} \tag{50}$$

where $c = \frac{\mu_+ - \alpha_i}{\Delta\alpha}$.

For the remaining terms we will use the following observation about linear interpolation.

Lemma 2 *Let f be a function, $x_i = i\Delta x$ and $a,b \in (x_i, x_{i+1})$. Let $\mathscr{I}f(a)$ and $\mathscr{I}f(b)$ be the approximations of $f(a)$ and $f(b)$ obtained by linear interpolation between $f(x_i)$ and $f(x_{i+1})$. Then*

$$\frac{\mathscr{I}f(b) - \mathscr{I}f(a)}{b-a} = \frac{f(x_{i+1}) - f(x_i)}{\Delta x}. \tag{51}$$

Proof We observe that $(a,\mathscr{I}f(a))$ and $(b,\mathscr{I}f(b))$ lie on the line segment from $(x_i,f(x_i))$ to $(x_{i+1},f(x_{i+1}))$. The slope of the line is given by either side of (51).

By Lemma 2 we have

$$\begin{aligned} \frac{\mathscr{I}g(s_{k-1},\mu_+) - \mathscr{I}g(s_{k-1},\mu_-)}{2\Delta s} &= \left(\frac{\mu_+ - \mu_-}{2\Delta s}\right)\frac{\mathscr{I}g(s_{k-1},\mu_+) - \mathscr{I}g(s_{k-1},\mu_-)}{\mu_+ - \mu_-} \\ &= \left(\frac{\mu_+ - \mu_-}{2\Delta s}\right)\frac{g(s_{k-1},\alpha_{i+1}) - g(s_{k-1},\alpha_i)}{\Delta\alpha} \end{aligned}, \tag{52}$$

as well as

$$\begin{aligned} \frac{\mathscr{I}g(s_k,\nu_+) - \mathscr{I}g(s_k,\nu_-)}{2\varepsilon\Delta s} &= \left(\frac{\nu_+ - \nu_-}{2\varepsilon\Delta s}\right)\frac{\mathscr{I}g(s_k,\nu_+) - \mathscr{I}g(s_k,\nu_i)}{\nu_+ - \nu_-} \\ &= \left(\frac{\nu_+ - \nu_-}{2\varepsilon\Delta s}\right)\frac{g(s_k,\alpha_{i+1}) - g(s_k,\alpha_i)}{\Delta\alpha} \end{aligned}. \tag{53}$$

Combining (49) with (50), (52) and (53) the NHDLH scheme can be written as

$$\begin{aligned} g'_{\mathrm{NHDLH}}(s_k,\alpha_{i+\frac{1}{2}}) &= (1-c)\,\frac{g(s_{k+1},\alpha_i)-g(s_{k-1},\alpha_i)}{2\Delta s} \\ &+ c\,\frac{g(s_{k+1},\alpha_{i+1})-g(s_{k-1},\alpha_{i+1})}{2\Delta s} \\ &+ \left(\frac{\mu_+-\mu_-}{2\Delta s}\right)\frac{g(s_{k-1},\alpha_{i+1})-g(s_{k-1},\alpha_i)}{\Delta\alpha} \\ &+ (1-\varepsilon)\left(\frac{\nu_+-\nu_-}{2\varepsilon\Delta s}\right)\frac{g(s_k,\alpha_{i+1})-g(s_k,\alpha_i)}{\Delta\alpha} \end{aligned} \tag{54}$$

with $c=\frac{\mu_+-\alpha_i}{\Delta\alpha}$. Recalling that $\mu_\pm=\mu(\pm\Delta s,\alpha_{i+\frac{1}{2}},\varepsilon)$ we obtain from (47) with $u=\pm\Delta s$ and $\alpha=\alpha_{i+\frac{1}{2}}$ that

$$c=\frac{\mu_+-\alpha_i}{\Delta\alpha}=\frac{1}{2}+\frac{\varepsilon\Delta s}{\Delta\alpha}-\frac{\Delta s^2}{2\Delta\alpha}(\varepsilon-1)^2\tan\alpha_{i+1/2}+\frac{\Delta s^3}{\Delta\alpha}d(\varepsilon,\alpha_{i+1/2})+O\left(\frac{\Delta s^4}{\Delta\alpha}\right) \tag{55}$$

as well as

$$\frac{\mu_+-\mu_-}{2\Delta s} \;=\; \varepsilon+d(\varepsilon,\alpha_{i+1/2})\Delta s^2+O(\Delta s^3). \tag{56}$$

Similarly, using (45) with $u=\pm\varepsilon\Delta s$ and $\alpha=\alpha_{i+\frac{1}{2}}$, one obtains

$$\frac{\nu_+-\nu_-}{2\varepsilon\Delta s} \;=\; 1-\frac{1}{2}\varepsilon^2\Delta s^2+O(\varepsilon^3\Delta s^3). \tag{57}$$

Combining (55) with Taylor expansions of the values of g about the point $(s_k,\alpha_{i+\frac{1}{2}})$ yields

$$\begin{aligned} &(1-c)\frac{g(s_{k+1},\alpha_i)-g(s_{k-1},\alpha_i)}{2\Delta s}+c\frac{g(s_{k+1},\alpha_{i+1})-g(s_{k-1},\alpha_{i+1})}{2\Delta s} \\ &= g_s+(2c-1)\frac{\Delta\alpha}{2}g_{s\alpha}+\frac{1}{8}\Delta\alpha^2 g_{s\alpha\alpha}+\frac{1}{6}\Delta s^2 g_{sss} \\ &\quad+\frac{2c-1}{12}\Delta s^2\Delta\alpha g_{sss\alpha}+O(\Delta\alpha^3+\Delta s^2\Delta\alpha^2+\Delta s^4) \\ &= g_s+\varepsilon\Delta s g_{s\alpha}-\frac{1}{2}\Delta s^2(\varepsilon-1)^2\tan(\alpha_{i+1/2})g_{s\alpha}+\frac{1}{6}\Delta s^2 g_{sss}+\frac{1}{8}\Delta\alpha^2 g_{s\alpha\alpha} \\ &\quad+O(\Delta s^3+\Delta\alpha^3). \end{aligned} \tag{58}$$

were the partial derivatives of g are evaluated at the point $(s_k,\alpha_{i+\frac{1}{2}})$. Similarly we obtain with (56)

$$\begin{aligned} &\left(\frac{\mu_+-\mu_-}{2\Delta s}\right)\frac{g(s_{k-1},\alpha_{i+1})-g(s_{k-1},\alpha_i)}{\Delta\alpha} \\ &= \left(\frac{\mu_+-\mu_-}{2\Delta s}\right)[g_\alpha(s_{k-1},\alpha_{i+1/2})+\frac{1}{24}\Delta\alpha^2 g_{\alpha\alpha\alpha}(s_{k-1},\alpha_{i+1/2})]+O(\Delta\alpha^4) \\ &= \left(\frac{\mu_+-\mu_-}{2\Delta s}\right)[g_\alpha-\Delta s g_{s\alpha}+\frac{1}{2}\Delta s^2 g_{ss\alpha}+\frac{1}{24}\Delta\alpha^2 g_{\alpha\alpha\alpha}(s_{k-1},\alpha_{i+1/2})] \\ &\quad+O(\Delta s^3+\Delta\alpha^2\Delta s+\Delta\alpha^4) \\ &= \varepsilon g_\alpha-\varepsilon\Delta s g_{s\alpha}+d(\varepsilon,\alpha_{i+1/2})\Delta s^2 g_\alpha+\frac{\varepsilon}{2}\Delta s^2 g_{ss\alpha}+\frac{\varepsilon}{24}\Delta\alpha^2 g_{\alpha\alpha\alpha} \\ &\quad+O(\Delta s^3+\Delta\alpha^2\Delta s). \end{aligned} \tag{59}$$

Finally we compute with the help of (57)

$$\begin{aligned}
&(1-\varepsilon)\left(\frac{\nu_+-\nu_-}{2\varepsilon\Delta s}\right)\frac{g(s_k,\alpha_{i+1})-g(s_k,\alpha_i)}{\Delta\alpha}\\
&=(1-\varepsilon)\left(\frac{\nu_+-\nu_-}{2\varepsilon\Delta s}\right)[g_\alpha+\frac{1}{24}\Delta\alpha^2 g_{\alpha\alpha\alpha}+O(\Delta\alpha^4)] \qquad (60)\\
&=(1-\varepsilon-\frac{1}{2}(1-\varepsilon)\varepsilon^2\Delta s^2)g_\alpha+(1-\varepsilon)\frac{1}{24}\Delta\alpha^2 g_{\alpha\alpha\alpha}+O(\Delta s^3+\Delta s^2\Delta\alpha^2+\Delta\alpha^4)
\end{aligned}$$

Combining the terms (58), (59), and (60) shows that under the hypotheses of Proposition 4 the NHDLH scheme, given by (54) equals

$$\begin{aligned}
&g'_{\mathrm{NHDLH}}(s_k,\alpha_{i+\frac{1}{2}})\\
&=g_s+g_\alpha+\Delta s^2\left[\frac{1}{6}g_{sss}-\frac{1}{2}(\varepsilon-1)^2\tan(\alpha_{i+1/2})g_{s\alpha}+(d(\varepsilon,\alpha_{i+1/2})+\frac{1}{2}(\varepsilon-1)\varepsilon^2)g_\alpha+\frac{\varepsilon}{2}g_{ss\alpha}\right]\\
&\quad+\Delta\alpha^2\left[\frac{1}{24}g_{\alpha\alpha\alpha}+\frac{1}{8}g_{s\alpha\alpha}\right]+O(\Delta s^3+\Delta\alpha^2\Delta s+\Delta\alpha^3).
\end{aligned}$$

6 Conclusions

This work explored the numerical implementation of a view dependent derivative that occurs in π-line reconstruction formulas for computed tomography. For two-dimensional fan-beam tomography a general description for various data acquisition geometries was reviewed. A detailed analysis was carried out for the specific case of a circular source curve and curved detector array. It included casting all schemes in a common framework and determining their leading error terms. The error terms provided an explanation for the lower accuracy of the direct scheme as well as the non-isotropic resolution of the NPH scheme. Conclusions drawn from the leading error terms were tested and confirmed with numerical experiments. The FHS, K, and NHDLH schemes yielded very similar reconstructions. While the K and NHDLH schemes do have additional error terms compared to the FHS scheme, these additional terms do not appear to be of practical concern.

The theory presented here does not cover flat detectors or elliptical source curves, which are subject of our future research. In our numerical experiments with a circular source curve the results for flat detectors were very similar to those for curved detectors. For an elliptical source curve the performance of the FHS and K schemes in our experiments was dependent on the particular alignment of the detector array. The FHS, K, and NHDLH schemes all gave good results when the detectors were oriented such that $\mathbf{e}_u(s)$ was perpendicular to $\mathbf{y}(s)$, while only the NHDLH scheme performed well when $\mathbf{e}_u(s)$ was oriented parallel to $\frac{d}{ds}\mathbf{y}(s)$.

References

1. Defrise, M., Noo, F., Clackdoyle, R., Kudo, H.: Truncated Hilbert transform and image reconstruction from limited tomographic data. Inverse Problems **22**(3), 1037–1053 (2006)
2. Faridani, A.: Fan-beam tomography and sampling theory. In: G. Olafsson, E.T. Quinto (eds.) The Radon Transform, Inverse Problems, and Tomography, *Proceedings of Symposia in Applied Mathematics*, vol. 63, pp. 43–66. American Mathematical Society, Providence, Rhode Island (2006)

3. Faridani, A., Hass, R., Solmon, D.C.: Numerical and theoretical explorations in helical and fan-beam tomography. Journal of Physics: Conference Series **124**, 012,024 (2008)
4. Hass, R., Faridani, A.: Regions of backprojection and comet tail artifacts for π-line reconstruction formulas in tomography. SIAM J. Imaging Sci. **5**(4), 1159–1184 (2012)
5. Herman, G., Naparstek, A.: Fast image reconstruction based on a Radon inversion formula appropriate for rapidly collected data. SIAM Journal on Applied Mathematics **33**(3), 511–533 (1977)
6. Izen, S.: Sampling in flat detector fan beam tomography. SIAM J. Appl. Math. **72**(1), 61–84 (2012)
7. Kak, A., Slaney, M.: Principles of computerized tomographic imaging. IEEE Press, New York (1988)
8. Kalender, W.: Computed Tomography: Fundamentals, System Technology, Image Quality, Applications, 3 edn. Publicis Publishing, Erlangen (2011)
9. Katsevich, A.: Theoretically exact filtered backprojection-type inversion algorithm for spiral ct. SIAM J. Appl. Math. **62**(6), 2012–2026 (2002)
10. Katsevich, A.: An improved exact filtered backprojection algorithm for spiral computed tomography. Advances in Applied Mathematics **32**, 681–697 (2004)
11. Katsevich, A.: A note on computing the derivative at a constant direction. Phys. Med. Biol. **56**, N53–N61 (2011)
12. Natterer, F.: The Mathematics of Computerized Tomography. Wiley, New York (1986)
13. Natterer, F.: Sampling in fan-beam tomography. SIAM J. Appl. Math. **53**(2), 358–380 (1993)
14. Natterer, F., Wübbeling, F.: Mathematical Methods in Image Reconstruction. SIAM, Philadelphia (2001)
15. Noo, F., Clackdoyle, R., Pack, J.: A two-step hilbert transform method for 2d image reconstruction. Phys. Med. Biol. **49**(17), 3903–3923 (2004)
16. Noo, F., Defrise, M., Clackdoyle, R., Kudo, H.: Image reconstruction from fan-beam projections on less than a short scan. Phys. Med. Biol. **47**, 2525–2546 (2002)
17. Noo, F., Hoppe, S., Dennerlein, F., Lauritsch, G., Hornegger, J.: A new scheme for view-dependent data differentiation in fan-beam and cone-beam computed tomography . Physics in Medicine and Biology **52**, 5393–5414 (2007)
18. Noo, F., Pack, J., Heuscher, D.: Exact helical reconstruction using native cone-beam geometries. Physics in Medicine and Biology **48**(23), 3787–3818 (2003)
19. Rieder, A., Faridani, A.: The semidiscrete filtered back projection algorithm is optimal for tomographic inversion. SIAM J. Numer. Anal. **41**(3), 869–892 (2003)
20. Zamyatin, A.A., Taguchi, K., Silver, M.: Practical Hybrid Convolution Algorithm for Helical CT Reconstruction . IEEE Trans. Nucl. Sci. **53**, 167–174 (2006)
21. Zou, Y., Pan, X.: An extended data function and its generalized backprojection for image reconstruction in helical cone-beam CT. Physics in Medicine and Biology **49**(22), N383–N387 (2004)
22. Zou, Y., Pan, X.: Exact image reconstruction on PI-lines from minimum data in helical cone-beam CT. Physics in Medicine and Biology **49**, 941–959 (2004)
23. Zou, Y., Pan, X., Sidky, E.: Image reconstruction in regions-of-interest from truncated projections in a reduced fan-beam scan. Physics in Medicine and Biology **50**(1), 13–27 (2004)